Title

Excited-state vibronic coherences and intramolecular charge transfer dynamics of the photoinactive cyanobacteriochrome NpF2164g5

Journal

The Journal of Chemical Physics, 164(9)

ISSN

0021-9606

Authors

Leslie, Chase H

Rockwell, Nathan C

Beck, Warren F

Publication Date

2026-03-07

DOI

10.1063/5.0305041

Peer reviewed

Excited-state vibronic coherences and intramolecular charge transfer dynamics of the photoinactive cyanobacteriochrome NpF2164g5

Chase H. Leslie,[1] Nathan C. Rockwell,[2] and Warren F. Beck [1, a)]

[1)]Department of Chemistry, Michigan State University, East Lansing, Michigan 48824 U.S.A.

[2)]Department of Molecular and Cellular Biology, University of California, Davis, Davis, California, 95616 U.S.A.

[a)]Corresponding author. Email: beckw@msu.edu

ABSTRACT

We have characterized the excited-state structural dynamics that follow optical excitation of the photoinactive cyanobacteriochrome (CBCR) NpF2164g5 to determine the first events along the photoisomerization reaction coordinate of the phycocyanobilin (PCB) chromophore in red-to-green photoactive CBCRs. Within 25 fs of photoexcitation to the first excited singlet state, S_1, a cross peak begins to develop below the diagonal of the broadband two-dimensional electronic spectrum (2DES) owing to the formation of a twisted conformation of the PCB chromophore with an enhanced intramolecular charge-transfer (ICT) character. Excited-state coherent wavepacket motions, including a torsion of the methine bridge between rings C and D and the carbon–hydrogen out-of-plane (HOOP) wagging vibration, are rapidly damped as the cross peak forms. This finding supports an assignment of the torsional and HOOP modes to the reaction coordinate of a coherent nonadiabatic mechanism. The ICT process is accompanied by an ultrafast Stokes shift and rapidly damped oscillations at the torsional mode's frequency, which are sensed by measurements of the energy gap of the cross peak using its first moment with respect to the detection frequency axis of the 2DES spectrum. These results have the further implication that polar side chains of nearby amino acid residues in the binding site of the PCB chromophore can manipulate the barrier height for photoisomerization in red-to-green photoactive CBCRs and in phytochromes by redistributing the π-electron density along the methine bridge between the C and D rings.

I. INTRODUCTION

An important and probably general feature of the excited-state potential energy surfaces of the electronic chromophores that undergo photoisomerization after $\pi \rightarrow \pi^*$ excitations is the presence of a low energy barrier on the resonant excited-state potential energy surface that divides planar and twisted

structures.[1–4] The excited-state dynamics are initially due to displacements from the Franck–Condon geometry principally with respect to the C=C and C–C bond stretching coordinates that modulate the bond-length alternation along the π-conjugated portion of the chromophore. Near the barrier, however, gradients along the vibrational coordinates with characters out-of-the-plane of conjugation are encountered, which project to lower energies towards a conical intersection (CI)[5,6] with the potential energy surface of the product. The twisted and bent structures that accompany progress along the photoisomerization reaction coordinate are likely to develop an intramolecular charge-transfer (ICT) character,[7,8] which can result in dynamical friction effects[9] on the rate and quantum yield of the photoproducts. In chromoproteins serving as photoreceptors, the presence of a barrier along the photoisomerization reaction coordinate offers a mechanism that can be used by the organism to regulate the sensitivity of the chromophore to the intensity and color of the incident light.[10]

In this contribution, we consider the properties of such a barrier that leads to control of the photoisomerization quantum yield in the cyanobacteriochromes (CBCRs),[11–14] which are cyanobacterial photoreceptor proteins with conserved GAF (cGMP-specific phosphodiesterase, cyanobacterial adenylate cyclase, and formate hydrogen lyase transcriptional activator FhlA) domains comparable to those of the phytochromes.[15] They sense the color and intensity of the ambient illumination using the ring-flipping photochemistry of their phycocyanobilin (PCB) (extended tetrapyrrole) chromophores.[16–22] Fig. 1 shows the structure of the CBCR NpR6012g4,[23] which exhibits a red-to-green photochromism.[18] The PCB-binding pocket in the GAF domain is constructed from a sheet of antiparallel β strands capped by a pair of α helices. The PCB chromophore is attached to the protein by a thioether linkage from a cysteine residue to ring A, the first of the four rings.

The resting, dark state of NpR6012g4, P_r, holds the PCB chromophore mainly in a planar conformation, with the D ring presented in the C15*Z*,*anti* configuration.[24] Upon absorption of red light, however, the PCB is converted with a 40% quantum

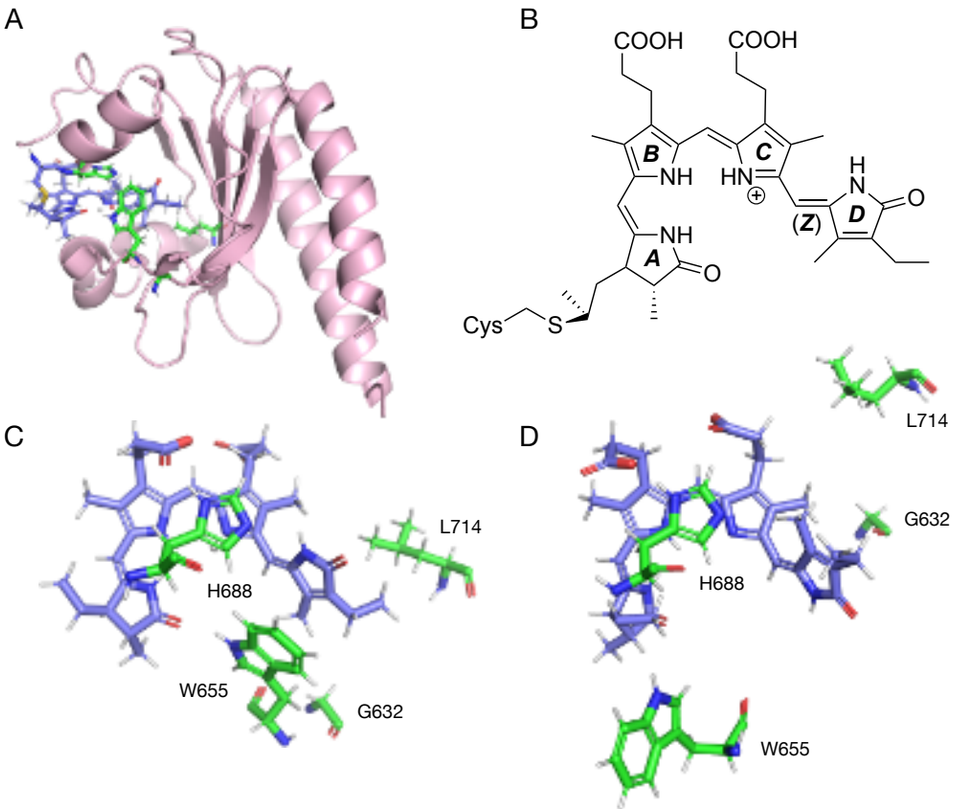

FIG. 1. (a) Structure of the dark-stable red state of the cyanobacteriochrome NpR6012g4, selected from the ensemble of NMR structures in pdb id 6BHN.[23] The phycocyanobilin chromophore and its thioether linkage to C687 are shown in blue, and the neighboring amino acid residues G632, H688, L714, and W655 are shown in green. (b) Structure of the phycocyanobilin chromophore in NpR6012g4 in the 15*Z* configuration. (c and d) Comparison of the structures of the phycocyanobilin chromophores of NpR6012g4 in the red 15*Z* and green 15*E* configurations, from pdb ids 6BHN and 6BHO, respectively.

yield[19] to a metastable, primary photoproduct, Lumi-R, which exhibits a ground-state absorption peak further to the red upon internal rotation of ring D.[18] On the ns–μs timescale, Lumi-R is subsequently converted to the green-absorbing form of the CBCR, P_g, due to conformational changes of the PCB chromophore and of the surrounding protein structure.[25] The P_g state presents the PCB chromophore in C15*E*,*anti* configuration.[24] The overall quantum yield of the photoconversion of NpR6012g4 from P_r to P_g is 32%,[18] much higher than the ~15% yield of the far-red photoproduct P_{fr} of the cyanobacterial phytochrome Cph1.[26–29] Comparison of the red and green structures of NpR6012g4[23] shown in Fig. 1c,d indicates that

the photochemistry also imparts an out-of-plane change of conformation of ring A relative to the coplanar B and C rings. An equivalent rotation of the A ring is observed in the crystal structure of CBCR Slr1393 from *Synechocystis* sp. PCC 6803.[22]

The rate and yield of the 15*Z*/15*E* photoconversion to the Lumi-R primary photoproduct of NpR6012g4 is determined by passage over an activation energy barrier (‡) on the S_1 potential energy surface. As shown in Fig. 2, the barrier divides the S_1 surface prior to a conical intersection (CI), where the potential energy surfaces of the 15*Z* and 15*E* configurations cross with respect to out-of-plane internal rotations of ring D of the PCB chromophore.[18] An analysis of resonance Raman intensities[30] and of the Lumi-R yields in femtosecond pump–dump experiments[31] indicates the presence of a comparable barrier in Cph1, which exhibits similar timescales for the excited-state dynamics.[19] Pump–dump experiments with NpR6012g4 have established that stimulated downward transitions from the potential-energy minimum prior to the excited-state barrier populate a metastable ground-state intermediate (GSI) with a partially photoisomerized configuration. Either the 15*Z* ground state or the 15*E* ground state can then be accessed thermally from the intermediate; this enhances the quantum yield for the Lumi-R photoproduct.[19,32] In contrast, the reverse 15*E*/15*Z* photoconversion is considered barrierless in truncated (Δ) preparations of Cph1 containing only the photosensory core;[27] coherent excited-state wavepacket motions on the S_1 potential energy surface of the PCB chromophore were observed with two-dimensional electronic spectroscopy (2DES) and femtosecond pump–probe spectroscopy directly from the Franck–Condon excited-state structure through the CI via a nonadiabatic mechanism.[33,34] 2DES was also used in studies of the bacteriophytochromes RpBphP2 from *Rhodopseudomonas palustris* and of PaBphP from *Pseudomonas aeruginosa* to probe the possible contribution of conformational inhomogeneity of the biliverdin-IXα chromophore in the photoisomerization kinetics.[35]

In this contribution, we discuss a series of broadband multidimensional electronic spectroscopy experiments characterizing the events that follow optical excitation

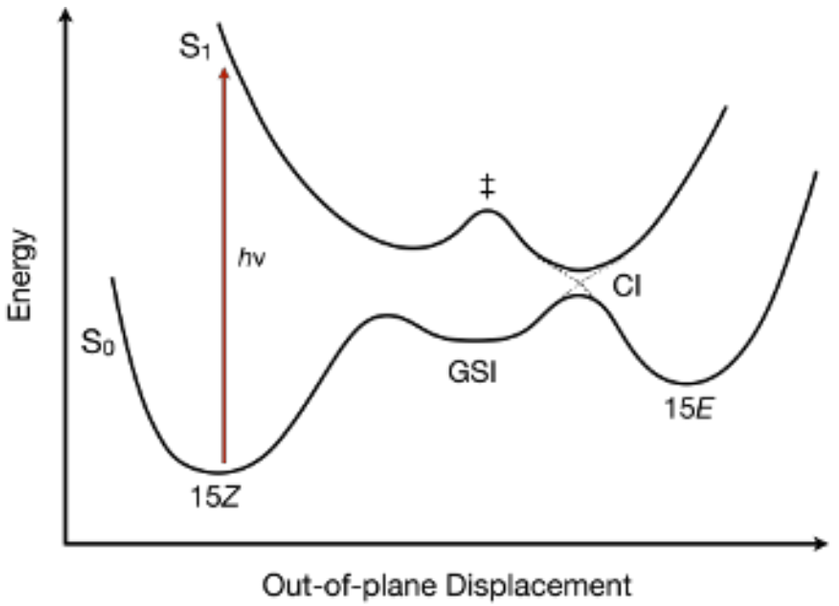

FIG. 2. Potential energy surfaces of the cyanobacteriochrome NpR6012g4 plotted with respect to out-of-plane displacements of the C_{15}=C_{16} methine linkage between rings C and D of the phycocyanobilin chromophore, after refs. 18 and 19. Optical preparation of the S_1 state from the 15*Z* ground state is followed by vibrational cooling and passage in >100 ps over an activation energy barrier, ‡, to reach the global excited-state minimum-energy structure. Branching to the 15*Z* and 15*E* (Lumi-R) configurations on the S_0 potential energy surface would then be obtained by passage through a conical intersection (CI), where the 15*Z* and 15*E* configurations are mixed. Pump–dump experiments[19,32] show that a partially isomerized ground-state intermediate (GSI) can be reached by a stimulated transition from the minimum prior to the transition-state barrier.

of the photoinactive CBCR NpF2164g5, which belongs to the same red-absorbing family of CBCRs as NpR6012g4 but does not yield the 15*E* ground state of the PCB chromophore upon illumination.[21] Rockwell et al.[36] showed that the G632V, H688Y, and L714F mutations of NpR6012g4 induce many of the properties of NpF2164g5, including an enhanced quantum yield of red fluorescence owing to inhibition of the photochemistry. Fig. 1a shows that the G632 and L714 sites are adjacent to ring D, suggesting that substitution with the more bulky side chains of valine and phenylalanine, respectively, would hinder its out-of-plane rotation. In the crystal structure of the CBCR AnPixJg2 from *Anabaena* sp. PCC 7120,[37] ring D is linked to the imidazole side chain of the corresponding residue H322 by a bridging hydrogen bond with the C ring's propionate group. Replacement with tyrosine would impart

a number of changes in the order around ring D, including also the packing of the conserved I691/L692 pair of residues and on the location of the tryptophan residue forming the "lid" of the binding site, W655.[37,38] Further, because the imidazole side chain of H688 is stacked with rings C and D of the PCB chromophore, there may be an additional impact on the photoisomerization reaction rate owing to a redistribution of the π-electron density of the PCB chromophore along its conjugated backbone. This type of electronic interaction[39] might contribute to the perturbed mid-visible circular dichroism spectrum observed upon replacement of the imidazole side chain with the phenol ring of a tyrosine residue in the H688Y mutant.[36]

The results presented here show that optical preparation of the S_1 excited state of NpF2164g5 is followed by ultrafast vibrational displacements of the PCB chromophore out of the plane of π conjugation, yielding an ICT state with a 25-fs time constant. A comparable intermediate would be expected prior to the barrier on the S_1 state potential energy surface in photoactive CBCRs as an excited-state counterpart to the GSI. Rapid damping of vibrational coherences assigned to torsional and carbon–hydrogen out-of-plane (HOOP) wagging modes of the methine bridge between rings C and D indicates that the ICT state is produced by coherent wavepacket motions from the Franck–Condon structure through a CI yielding the product ICT state prior to the excited-state barrier. The predominantly torsional character of the reaction coordinate is revealed by an underdamped response of the protein and solvent surroundings, which is detected by a first-moment (FM) analysis of the below-diagonal cross peak in the two-dimensional electronic spectrum (2DES) due to the ICT state. These results suggest that the kinetics of photochromism in CBCRs and likely also in phytochromes are rate and yield limited by the formation of the ICT state, which would control the height of the activation energy barrier and the extent of the reorganizational response of the surrounding binding site and aqueous medium.

II. EXPERIMENTAL

Sample Preparation

NpF2164g5 was prepared by the Lagarias laboratory at the University of California, Davis, using previously published protocols.[11,18,21,36,40] Samples of NpF2164g5 were stored at −80 °C suspended in a buffer solution at pH 7.8 containing 25 mM N-[*tris*(hydroxymethyl)methyl]-2-aminomethanesulfonic acid (TES)–KOH, 100 mM KCl, and 10% (v/v) glycerol as a cryoprotectant. For use in the work reported here, the samples were thawed in darkness and then the buffer solution was exchanged with a 10-mM sodium phosphate–NaOH buffer solution at pH 7.4 by repeated concentration in an Amicon ultrafiltration cell over a Millipore YM10 membrane. For low-temperature fluorescence measurements, glycerol was added to the solution to make a 60:40 glycerol:buffer mixture, which obtains clear glasses at cryogenic temperatures.

Linear Absorption and Fluorescence Spectroscopy

Fluorescence spectra were recorded as discussed previously with a home-built fluorescence spectrometer.[41] The excitation light source was a broadband LED (Thorlabs M530L4) filtered by a double monochromator (Spectral Products AG1200-00500-303) operated in an additive configuration, with a spectral bandpass of 2 nm. Fluorescence emission with magic-angle polarization was detected with a 4-nm spectral bandpass by an Acton Research SP-150 spectrograph and a Oxford Instruments Andor Newton 940-BV CCD detector. The excitation monochromator and emission spectrograph were calibrated with an Ocean Optics HG-1 lamp; the absolute spectral response of the detection system was calibrated with an Ocean Optics HL-3 plus-CAL reference lamp. The apparatus was controlled by LabVIEW (National Instruments) routines. The sample was held in a fused silica cuvette with a 1-cm optical path length, which was mounted in a sample-in-exchange-gas liquid nitrogen

cooled cryostat (Oxford Instruments OptistatDN, with a MercuryiTC temperature controller).

Reference absorption spectra were measured in a Shimadzu UV-2600 spectrometer at ambient temperature (293 K). An additional series of absorption spectra were recorded over the 80–298 K range using the Oxford cryostat with a single-beam, fiber-optic absorption spectrometer employing a compact spectrograph/CCD detector, which was described previously.[42]

Multidimensional Electronic Spectroscopy

Broadband two- and three-dimensional electronic spectra (2DES and 3DES) were recorded at ambient temperature (293 K) with the spectrometer described previously,[43,44] which employs a two-beam, pump-probe optical configuration with the use of adaptive pulse shaping[45] and phase-sensitive detection.[46] Both beams are obtained from a noncollinear optical parametric amplifier (NOPA), which is pumped by an amplified Yb laser with a 100-kHz repetition rate. The first two excitation pulses in the stimulated photon-echo pulse sequence used in 2DES spectroscopy[47,48] are prepared from a single incident pulse by the pulse shaper in the pump beam, which scans the coherence time interval between the two pulses, τ, from 0 fs to 50 fs with 0.5 fs steps. The τ scan obtains the excitation axis of the 2DES spectrum after Fourier transformation of the detected signal amplitude. A broadband achromatic half-wave retarder plate in the pump beam is used to rotate its plane of polarization to the magic angle, 54.7°, relative to that of the probe beam.[44] The waiting time interval between the second of the two excitation pulses and the delayed probe pulse, T, is scanned with a conventional time-of-flight delay line. The detection axis of the 2DES spectrum is determined directly from the intensity of the probe pulse after it passes through the sample, as measured by a home-built spectrograph and a CCD detector. The zero-of-time for the T axis was determined with spectral interferometry.[49,50] Owing to the use of the pulse shaper approach, the

2DES spectra presented here are purely absorptive (lacking dispersion content).[45] Because phase cycling of the two excitation pulses was not performed with the pulse shaper, however, the 2DES amplitudes are the sum of those from the rephasing and nonrephasing nonlinear optical response pathways.[51]

At the sample position, the measured laser pulse duration determined by MIIPS scans[52] was 7.2 fs. The pulse energy for each of the three laser pulses in the stimulated photon echo sequence was 5 nJ, with a 100-kHz repetition rate, giving an average incident power of 1.5 mW. The diameters of the pump and probe spots overlapped on the sample were measured with a beam profiling camera to be ~100 μm. Figs. 1–3 in the Supplementary Material show a SHG-FROG spectrogram,[53] an interferometric autocorrelation signal, and residual phase plots for the pump and probe beams, which were measured using the pulse shapers. The NpF2164g5 samples were diluted with additions of the phosphate buffer solution to obtain an absorbance of 0.12 at 642 nm in a fused silica flow cell with a 1-mm optical path length. The sample was recirculated through the sample cell during the experiment by a peristaltic pump. Control 2DES spectra from water blanks and from methylene blue samples in water solvent, presented as Fig. 4 in the Supplementary Material, were recorded using similar experimental conditions. These spectra were used to characterize the instrument response function and the extent of background 2DES signals near $T = 0$ fs.

Global and target models of the 2DES spectra were determined with the CarpetView program (Light Conversion). The instrument-response function width used in these models, 12 fs, is consistent with the assumption of Gaussian electric field profiles for the 7-fs pulses and results in rise times for signal amplitudes consistent with those observed in controls and the decay of the nonresonant signal observed in the water blanks. To mitigate the effects from the temporal overlap of the pump and probe pulses near the zero-of-time of the delay T axis, the global models truncate data points prior to $T = 5$ fs, but the same global model parameters

and evolution-associated difference spectra (EADS) are obtained with truncation at $T = 15$ fs.

Linear prediction, singular value decomposition (LPSVD) models of coherences[54–56] were obtained with a Julia program we adapted from the MATLAB code supplied by Champion and coworkers.[57,58] The $T < 10$ fs range of 2DES transients were excluded from the LPSVD models. Power spectra were calculated using the fitted amplitudes and damping times from the LPSVD models using normalized Lorentzian line shapes, which allows one to compare them with Fourier transform power spectra.

III. RESULTS AND DISCUSSION

Linear absorption and fluorescence spectra

The linear absorption and fluorescence oscillator strength spectra of NpF2164g5 shown in Fig. 3 exhibit a partially resolved vibronic progression with respect to several vibrational modes of the PCB chromophore. At cryogenic temperatures, the absorption line shape narrows markedly to reveal the contribution of a low-frequency mode to the main, 0–0 vibronic band, and a shoulder appears prior to the 0–1 vibronic satellite. The absorption and fluorescence spectra deviate markedly from mirror symmetry at 80 K, as shown in Fig. 3, which indicates that the PCB chromophore undergoes an excited-state change in its electronic structure prior to vibrational equilibration. At 298 K, the asymmetry is less apparent, but the 0–0 and 0–1 peaks of the fluorescence spectrum are narrower than those of the absorption spectrum.

Numerical simulations employing the multimode Brownian oscillator (MBO) model[59–62] obtain an approximate description of the absorption and fluorescence spectra by incorporating progressions at four vibrational frequencies, at 350, 800, 1320, and 1610 cm^{-1}. A 350-cm^{-1} mode was not included in the prior simulations of the absorption spectrum of Cph1 using stimulated resonance Raman intensities,[30]

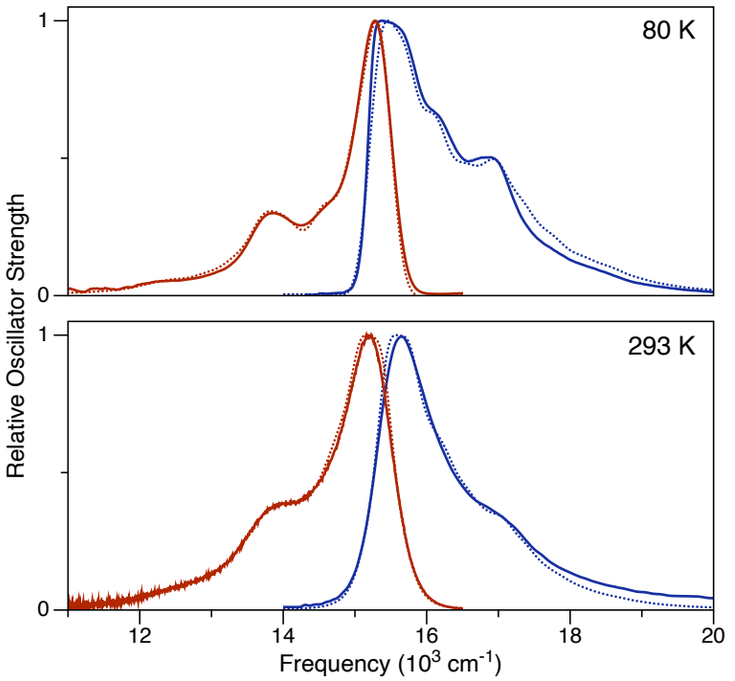

FIG. 3. Absorption (blue) and fluorescence (red) spectra of the cyanobacteriochrome NpF2164g5 recorded at 80 K and at 293 K, plotted superimposed with numerical simulations using the multimode Brownian oscillator (MBO) model (dashed). The spectra are plotted as the oscillator strengths $\varepsilon(\nu)/\nu$ and $\lambda^2 F(\nu)/\nu^3$, respectively, with normalization to their peak maxima. The sample used for the spectra recorded at 80 K was suspended in a 60:40 glycerol:buffer solution mixture to obtain a clear glass. The excitation light source for the fluorescence spectra at 80 K and 293 K was tuned into the vibronic satellite peak in the absorption spectrum at 17100 cm^{-1} (585 nm) and 17240 cm^{-1} (580 nm), respectively. Fig. 5 in the Supplementary Materials compares the 80-K absorption spectrum with additional spectra recorded with the same sample at 160, 240, and 293 K. The model spectra incorporate four underdamped vibrational modes of the bilin chromophore, with natural frequencies of 350, 800, 1320, and 1610 cm^{-1}. The model parameters are tabulated in the Supplementary Materials as Tabs. I–IV.

but it is required here to handle the low-frequency feature observed in the absorption spectrum at 80 K, and it is observed directly in excited-state vibrational coherences, as discussed below. Considering the character of analogous vibrational modes observed in styrene,[63–65] the character of this mode is likely a pyramidalizing, concerted twisting and bending motion of the methine linkage between rings C and D of the PCB chromophore. The three higher frequencies used in the MBO model correspond to the HOOP mode, to the C–C and N–H vinyl rocking motions, and to

the local C=C and C=N stretching vibrations, respectively. These frequencies are observed in resonance Raman[66] and femtosecond stimulated Raman[26,30] spectra of Cph1 and of AnPixJg2.[67] Note that the stimulated Raman spectrum of Cph1 also exhibits less intense peaks in the 400–500-cm^{-1} range that are attributed to vinyl C=C torsional modes, and there is a 664-cm^{-1} Raman feature associated with coupled torsions of C=C and C–C bonds, also likely derived from the methine linkage between rings C and D.[30,68]

The model parameters listed in Tabs. I–IV in the Supplementary Materials suggest that the PCB chromophore undergoes an excited-state change in its electronic structure due to an out-of-plane twisting or bending distortion of its π-conjugated framework. The reorganization energies for the four modes in the model for the absorption spectra give projections for a harmonic potential energy surface from the Franck–Condon structure on the S_1 surface, whereas the reorganization energies for the fluorescence spectrum are those for a harmonic potential energy surface for the emissive structure reached following the excited-state motions and after vibrational equilibration. At 80 K, the reorganization energies of the 350- and 800-cm^{-1} modes are much smaller for the fluorescence spectrum than those for the absorption spectrum, which raises the possibility that out-of-plane twisting or bending motions of ring D are hindered by the frozen solvent and protein surroundings. At 293 K, the fluorescence spectrum is modeled by a smaller reorganization energy for the HOOP mode but a larger reorganization energy is obtained for the 1320-cm^{-1} mode, which suggests that the C=C double bond character of the methine linkage is redistributed compared to that of the equilibrium ground-state structure. The parameters for the 80- and 293-K absorption spectra are not identical, which further suggests that the PCB chromophore adopts a somewhat different ground-state structure at low temperatures in the presence of glycerol. Not considered here, owing to the likelihood that the PCB chromophore exhibits a non-planar conformation in the electronic ground state, is the possibility that a Herzberg–Teller coupling[69–71]

contributes to deviations from mirror symmetry of the absorption and fluorescence lineshapes.

2DES spectra

Fig. 4 shows a series of snapshots of the broadband 2DES spectra recorded with NpF2164g5 at room temperature as a function of the pump–probe delay time T reaching out to 500 fs. A cross peak develops below the diagonal of the 2DES over $T < 100$ fs due to the ultrafast formation of an excited-state structural intermediate. The cross peak is parallel to the diagonal in the $T = 5$-fs spectrum, but at $T = 50$ fs it is aligned along the detection axis, just to the blue of the peak maximum of the fluorescence spectrum. An approximate description of the principal nonoscillatory components arising from population signals in the 2DES spectra is obtained with a global model[72] incorporating only two spectrokinetic species, for the optically prepared, Franck–Condon excited state on the S_1 potential energy surface and an excited-state product due to a nonradiative decay process with a 25-fs time constant. Fig. 5 shows the two-dimensional evolution-associated difference spectra (EADS) for the two species, which represent the 2DES spectrum for a given species averaged over the ensemble. Note that the response detected at longer delays in femtosecond pump–probe experiments[21] requires a more complicated global model to handle heterogeneity in the kinetics, especially in the ground-state recovery time constant.

The EADS for the initial, optically prepared spectrokinetic species in the global model, $S_1/15Z$, displays a pattern of alternating bands arising from positive amplitudes from ground-state bleaching (GSB) and stimulated-emission (SE) pathways flanked by negative amplitudes due to excited-state absorption (ESA) pathways. The GSB part of this pattern corresponds to the vibrational progression displayed by the linear absorption spectrum; this is consistent with large structural displacements of the PCB chromophore from the Franck–Condon geometry, as discussed above and noted previously in 2DES studies of the Cph1Δ system.[33,34] The spectral line shapes

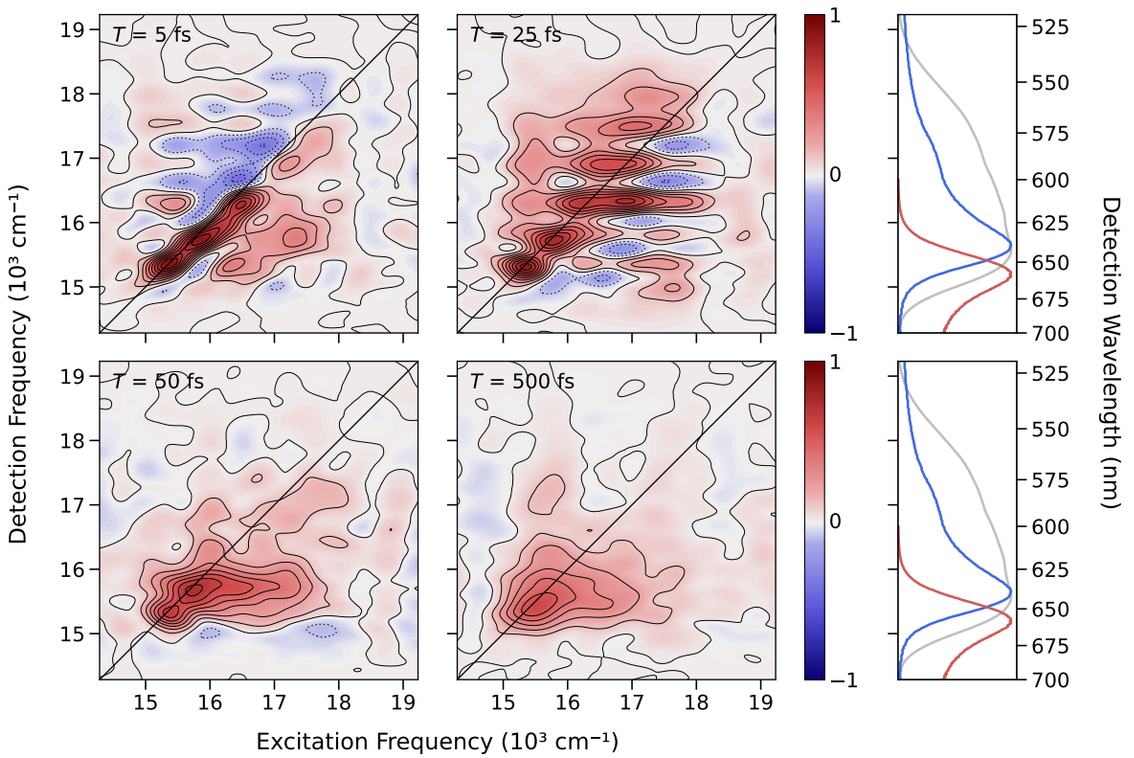

FIG. 4. 2DES spectra of NpF2164g5 with snapshots selected at four probe delays T. The side panels reproduce from Fig. 3 the absorption (blue) and fluorescence (red) oscillator strength spectra and the laser intensity spectrum (grey). The contours of the 2DES spectra are shaded with respect to the color bars drawn to the right, which indicate the maximum and minimum amplitude in the 2DES data set.

observed here in the 2DES spectra are narrowed, providing resolution of vibronic structure at short delays T, owing to the use of excitation pulses that are much shorter than the pure inhomogeneous broadening timescale. A broad ESA band is superimposed, as previously detected in pump–probe spectra of bilin proteins, such as those of the single PCB-containing α subunit of C-phycocyanin.[73] The net ESA band of NpF2164g5 was observed previously[21] to extend over the 410–550-nm range. This is consistent with the net ESA band observed here in the 2DES spectra at short delays T above the diagonal.

The EADS of the product compartment in the global model exhibits a cross peak arising mainly from SE pathways. We label this intermediate as S_1/ICT given the inference below that this state develops ICT character due to out-of-plane

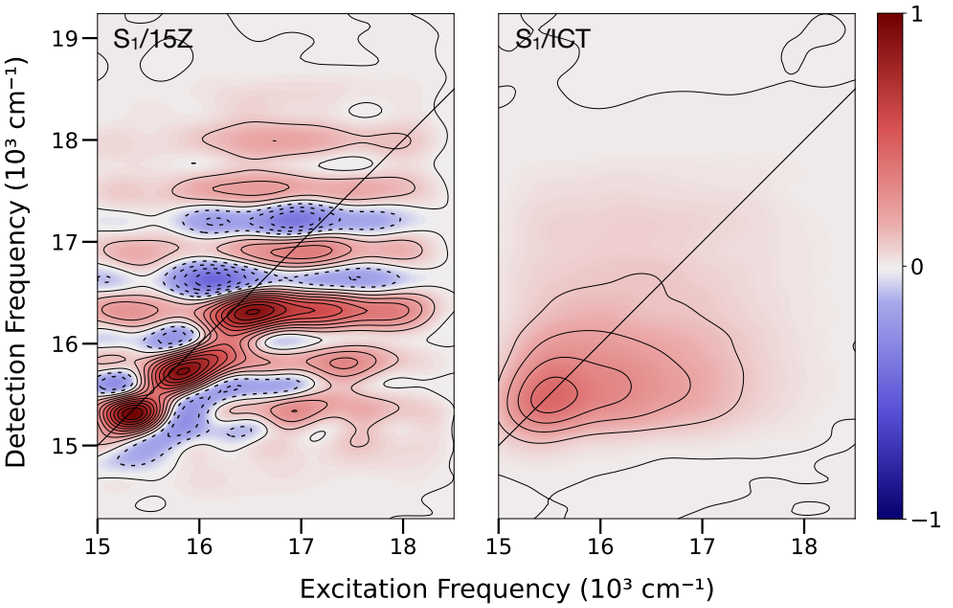

FIG. 5. Evolution-associated difference spectra (EADS) for a two-dimensional global model for the 2DES spectra of NpF2164g5. *Left*: EADS for the Franck–Condon $S_1/15Z$ state, as produced by absorption transitions from the $S_0/15Z$ ground state. *Right*: EADS for the S_1/ICT product state, as produced by nonradiative decay from the $S_1/15Z$ state with a 25-fs time constant. The lifetime of the S_1/ICT state for recovery to the original ground state is 2.1 ps. The global model selects the 15000–18500-cm^{-1} range of the excitation frequency axis and the $T > 10$-fs probe delay range of the 2DES data set. The EADS for a one-dimensional global model of the excitation slice of the 2DES spectrum at 16400 cm^{-1} is shown in the Supplementary Material as Fig. 6.

deformations of ring D of the PCB chromophore with respect to the methine bridge between rings C and D. Extensive broadening of the GSB and SE character along the antidiagonal direction of the EADS indicates that conversion to the ICT state accompanies essentially a complete loss of memory of the Franck–Condon energy gap, but the persistence of the GSB spanning the diagonal reports that the initial and product states share the same electronic ground state. The lack of net ESA character in the EADS of the product ICT state is further evidence for a significant structural displacement from the Franck–Condon geometry because the energy gaps for stimulated transitions to higher singlet electronic states are apparently being shifted to the red, out of the probed spectral range. This sort of spectral evolution has been observed previously in the ketocarotenoid canthaxanthin, where the overlapping

GSB/SE and ESA transitions from the resonant S_2 state are replaced on an ultrafast time scale by the SE cross peak from the S_x intermediate.[44] The 25-fs time constant in the present case is comparable to the vibrational periods of the C=C and C=N stretching modes of the PCB chromophore but well shorter than the usual timescale expected for vibrational dephasing, ~1 ps, which anticipates that the intermediate is formed by a vibrationally coherent process.

Analysis of coherences

The amplitude of the 2DES spectrum of NpF2164g5 is deeply modulated with respect to the delay T axis at a number of the vibrational frequencies of the PCB chromophore over the 200–1600-cm^{-1} range. The oscillation maps shown in Fig. 6 report the Fourier transform (FT) power spectrum of the modulated 2DES amplitudes as a function of the detection frequency for the excitation energy slice of the 3DES spectrum near the center of the cross peak, at ~16400-cm^{-1}. The peak pattern in these maps arises from a superposition of the signals arising from rapidly damped excited-state and slowly damped ground-state wavepacket motions. The latter arise from stimulated Raman pathways,[74,75] which contribute progressions[70,76–78] in the oscillation map for the T = 50–300-fs window in the right-hand panel of Fig. 6. The peaks at several of the coherence frequencies exhibit spacings along the detection axis matching the mode frequency, although those for lower frequency coherences may also indicate the presence of combinations.[78] The oscillation map for the T = 5–100-fs window shown in the left-hand panel, however, is dominated by rapidly damped modulations due to the vibrational coordinates that promote nonradiative decay. The 3DES integrated vibronic spectrum[70,79] shown as Fig. 7 in the Supplementary Materials retrieves peaks corresponding to many of the normal modes of the PCB chromophore by averaging the oscillation maps over the entire range of excitation frequencies of the 2DES spectrum.

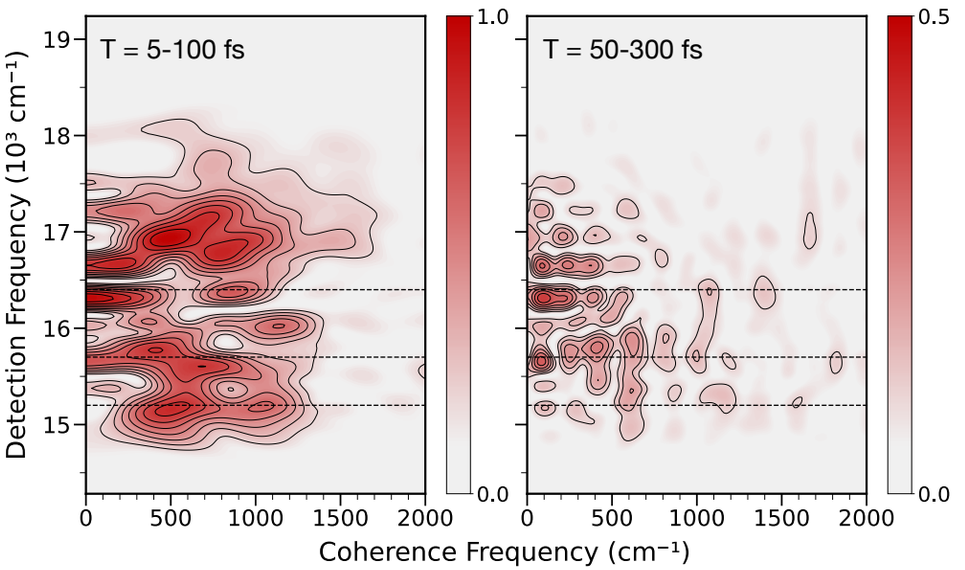

FIG. 6. Oscillation maps for coherences in the 2DES spectrum of NpF2164g5 at the 16400 ± 200-cm^{-1} slice of the excitation axis. *Left*: for the T = 5–100 fs window of the delay T axis. *Right*: for the T = 50–300 fs window of the delay T axis. As indicated by the color bars for the Fourier amplitudes, the full scale of the T = 50–300 fs map is half of that of the T = 5–100 fs map. The dashed lines drawn across the oscillation map mark the detection frequencies at which the three transients shown in Fig. 7 are sampled.

The most intense amplitude modulations observed in the 2DES spectrum of NpF2164g5 are due to excited-state wavepacket motions with two characteristic damping times, ~25 fs and ~200 fs, with the latter observed only at low detection frequencies, near the maximum of the fluorescence spectrum. Fig. 7 compares amplitude transients sampled for the excitation frequency of 16400 cm^{-1} at detection frequencies near the diagonal of the 2DES spectrum, in the center of the cross peak, and near the fluorescence emission maximum. These transients characterize the decay of population in the optically prepared S_1 state and the rise of population in the ICT state. Modulated residual waveforms are then obtained by subtracting the nonoscillatory part of the 2DES signal amplitude, which was estimated using the 2D global model. Linear prediction, singular value decomposition (LPSVD)[54–58,80] models for the residuals at the diagonal and at the cross peak retrieve approximate models for the residual waveforms with two principal components, at modulation frequencies of ~300 cm^{-1} and ~800 cm^{-1}. The ~300 cm^{-1} component is the

most intense of the two components observed in the diagonal transient, so one would attribute it to the out-of-plane 350-cm^{-1} mode discussed above, whereas the amplitude of the ~800 cm^{-1} component is enhanced at the cross peak, where the two components make roughly equal contributions. The damping time constant for both of the components in the LPSVD models is ~25 fs. The damped cosinusoidal modulation observed at the cross peak is delayed by ~20 fs from that at the diagonal, as judged by the timing of the positive recurrences in the two residuals at ~45 fs and ~25 fs, respectively. These parameters for the excited-state wavepacket motion should be regarded as crude estimates with perhaps ±10-fs confidence intervals, given the ~12-fs instrument-response width of the current experiments obtained with the use of ~7.2-fs excitation laser pulses.

Based on these observations of excited-state wavepacket motions, Fig. 8 proposes a vibrationally coherent, nonadiabatic mechanism for the nonradiative conversion of the S_1 state of NpF2164g5 to the ICT state after photoexcitation from the 15*Z* minimum of the ground state. The potential energy diagram shown here describes the hypothesis that the S_1 and ICT states interact at a CI, where transitions between the reactant and product states are the most probable. The role of CIs in sub-ps nonradiative processes in organic molecules has been extensively discussed,[2,5,81–84] and there have been recent experimental and theoretical investigations of CIs in studies of materials[85] and from this laboratory of light-harvesting proteins[43,86,87] and in semiconductor QDs.[88,89] Owing to its out-of-plane character, as discussed earlier in the assignment of the linear absorption spectrum, we suggest that displacements along the coordinates of the ~350-cm^{-1} vibrational mode would promote the induction of a zwitterionic electron configuration, due to ICT across the C=C bond[7,8,90–92] in the methine linkage between the C and D rings.

The 350-cm^{-1} and 800-cm^{-1} modes are good candidates for the branching (or tuning and coupling) coordinates, which control the energy gap and the extent of mixing of the diabatic states at a CI,[81,93] because these two modes are damped on the same timescale as the formation of the product state. This relationship between

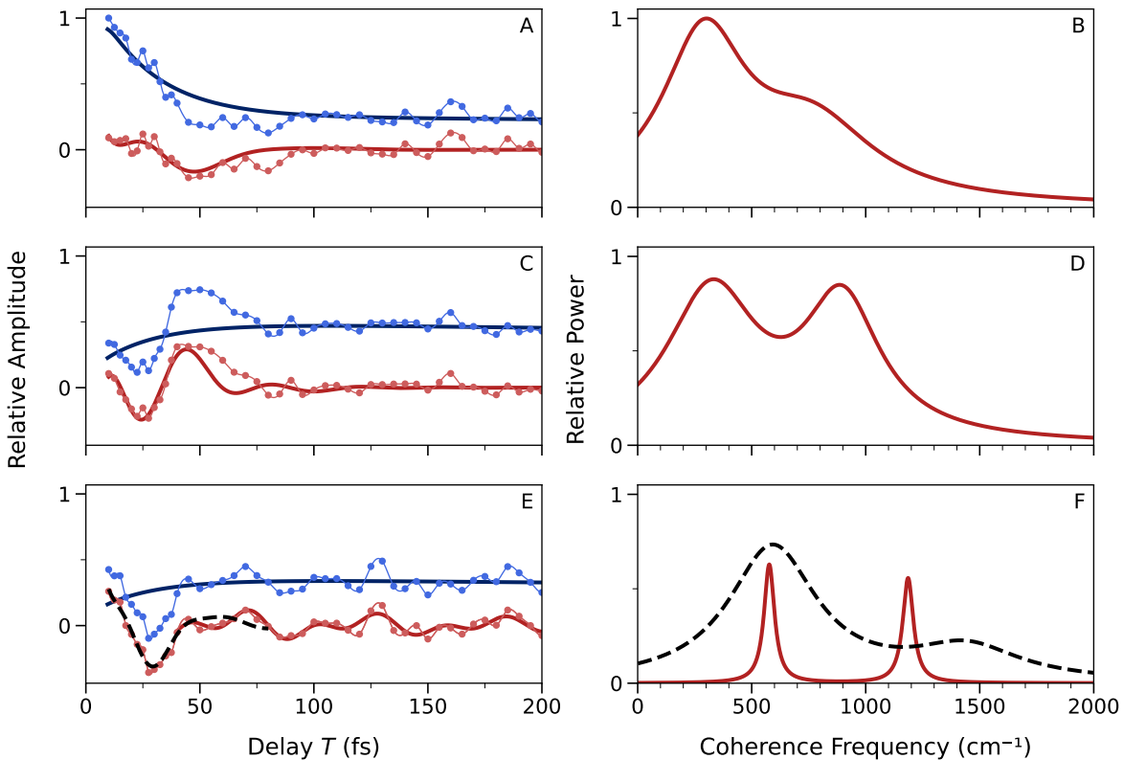

FIG. 7. Amplitude transients (blue dots) sampled from the 2DES spectrum of NpF2164g5 at the excitation frequency of 16400 cm^{-1} at three detection frequencies: (a) near the diagonal at 16230 cm^{-1}; (c) in the below-diagonal cross peak at 15700 cm^{-1}; and (e) near the fluorescence maximum at 15300 cm^{-1}. Each transient is superimposed with the fitted amplitude (dark blue) from an overdetermined global model, which estimates the nonoscillatory background at each coordinate. The residual transient (data − fit, red dots) is shown in (a), (c), and (e) with fitted curves (dark red and black dashed) determined by linear prediction, singular value decomposition (LPSVD) models, which are plotted as the power spectra in panels (b), (d), and (f), respectively. The LPSVD models in panel (e) are provided for two time windows, T =5–80 fs (black dashed) or T =40–200 fs (red). The ordinates for the amplitude transients and power spectra employ the same relative scaling. The fit parameters for the LPSVD models are reported in the Supplementary Materials as Tables V–VIII.

the rate of decay for a nonradiative process and the damping times for wavepacket motions through the CI has been noted in several systems.[94-96] A theoretical discussion of this phenomenon suggests[97] that it arises from a *quantum quench*,[98] an instantaneous change in the electronic structure upon crossing through the CI, which would result in new forces and changes in vibrational displacements. The vibrations attributed to the branching coordinates for the CI for the photoisomerization of retinal in rhodopsin[99-101] are analogous but exhibit higher natural frequencies than

those in NpF2164g5 because for the latter the character of motion includes ring D of the PCB chromophore.

In addition to rapidly damped modulations at short delays T, the amplitude transient sampled at low detection frequencies near the fluorescence maximum, Fig. 7e, carries a slowly damped modulation that is not observed at higher detection frequencies. The LPSVD model for the T = 40–200-fs window of the transient retrieves principal components at 600-cm^{-1} and 1200-cm^{-1}. These are likely to be from spectator modes, which apparently do not suffer fast decoherence due to the crossing to the ICT state.[102] The alternative assignment that these coherences arise from impulsive formation of the ICT state is not satisfactory given that the time constant for the process is comparable to the oscillatory periods of these modes. Further, the ~200-fs damping time constants for these components is consistent with the the rate of intramolecular vibrational redistribution (IVR), the *incoherent* transfer of vibrational energy to other modes of the PCB chromophore that serve as a proximal bath prior to dissipation to the surrounding medium.[80,103] These motions would be principally detected after crossing of wavepackets from the resonant Franck–Condon state and as they undergo cooling near the bottom of the potential energy surface of the ICT state.

Fig. 8 also indicates that stimulated Raman pathways will launch slowly damped coherent wavepacket motions on the electronic ground state. As noted above, this mechanism is expected to contribute a regular progression of peaks spaced by the mode frequency along the detection axis of an oscillation map,[76,77] but the superimposed modulation pattern from the excited-state modes is evidently much more intense in the present case. This observation is consistent with theory for broadband pump–probe spectroscopy discussed by Pollard and Mathies.[75] As a rule of thumb, the amplitude of the modulations due to ground-state wavepacket motions is optimized when the duration of the excitation pulses is about one-third the vibrational period of a given mode. In the present experiments, stimulated Raman coherences of the PCB chromophore with natural frequencies below 1600 cm^{-1} are

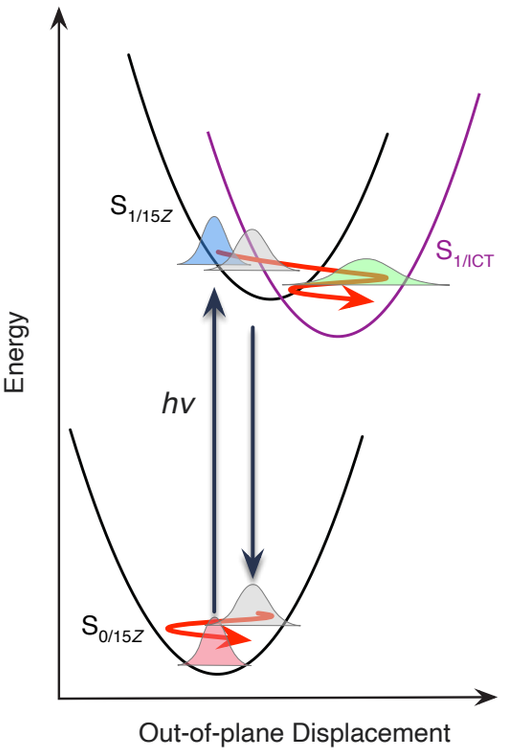

FIG. 8. Coherent nonadiabatic mechanism yielding an ICT state in NpF2164g5 following optical preparation of the S_1 state from the $15Z$ minimum of the S_0 state. The excited-state potential energy surfaces shown here correspond to the $15Z$ region of the excited-state potential energy surface shown in Fig. 2, prior to the activation barrier. excited-state wavepacket motions travel from the Franck–Condon structure (blue wavepacket) to the ICT state by passing through a conical intersection. ground-state wavepacket motions arise from stimulated Raman pathways resulting from an instantaneous displacement (gray wavepackets) from the Franck–Condon structure.

increasingly attenuated by the use of ~7-fs laser pulses as the frequency decreases. The damping time of these coherences would be expected to be >500 fs, longer than those of either class of excited-state wavepacket motions.

First moment analysis

If the intermediate detected in the time evolution of the 2DES spectrum really arises from an ICT state, one would expect to observe a dynamic Stokes shift of the energy gap for SE transitions by the PCB chromophore on an ultrafast time scale. The SE signal would shift to lower detection frequencies owing to a

solvation or reorganizational response of the protein- and aqueous solvent-derived medium[73,104–107] to the formation of an enhanced permanent dipole moment for the PCB chromophore in the ICT state. This response can be detected using information in the 2DES spectrum by measuring $\langle \nu_{\mathrm{det}} \rangle$, the average detection frequency of a slice of the cross peak along the detection axis:

$$\langle \nu_{\mathrm{det}} \rangle = \frac{\int_{\nu_1}^{\nu_2} \mathrm{d}\nu_{\mathrm{det}}\, \nu_{\mathrm{det}} A(\nu)}{\int_{\nu_1}^{\nu_2} \mathrm{d}\nu_{\mathrm{det}}\, A(\nu)} \tag{1}$$

The denominator of Eq. 1 normalizes the first moment integral, $\int \mathrm{d}\nu_{\mathrm{det}}\, \nu A(\nu)$, with the corresponding integral over the cross peak's amplitude, $\int \mathrm{d}\nu_{\mathrm{det}}\, A$. The response measured with $\langle \nu_{\mathrm{det}} \rangle$ is accordingly not directly sensitive to the delay T kinetics of the signal amplitude, which is also the case in measurements of the stimulated photon-echo peak shift (3PEPS).[60,108,109] If the cross peak is not fully resolved from the diagonal of the 2DES spectrum, the average value reached at long delays T will be determined by the specific choice of the integration limits ν_1 and ν_2, but the dynamics information returned by the shift of $\langle \nu_{\mathrm{det}} \rangle$ as a function of the delay T is robust.

The top panel of Fig. 9 shows the time evolution of the cross peak in the 2DES spectrum at the 16400 cm^{-1} excitation energy slice in terms of a heat map, with the amplitude color coded just as the 2DES spectra are in Figs. 4 and 5. Inspection reveals an overall red shift of the amplitude maximum accompanying a rapidly damped oscillation. The bottom panel of Fig. 9 shows the $\langle \nu_{\mathrm{det}} \rangle$ response evaluated over the detection frequency range of the cross peak shown in the heat map. The response includes a net ~60-cm^{-1} red shift of the cross peak with a Gaussian temporal profile accompanying the 25-fs rise of population in the nonradiative decay intermediate of NpF2164g5. The ~50-fs time constant may correspond to that of the inertial part of the solvation response,[60,110] whereas the diffusive, reorganizational response would be expected to occur over a longer timescale than measured here, with some relaxation components in the ns range.[73,111] Femtosecond time-resolved fluorescence

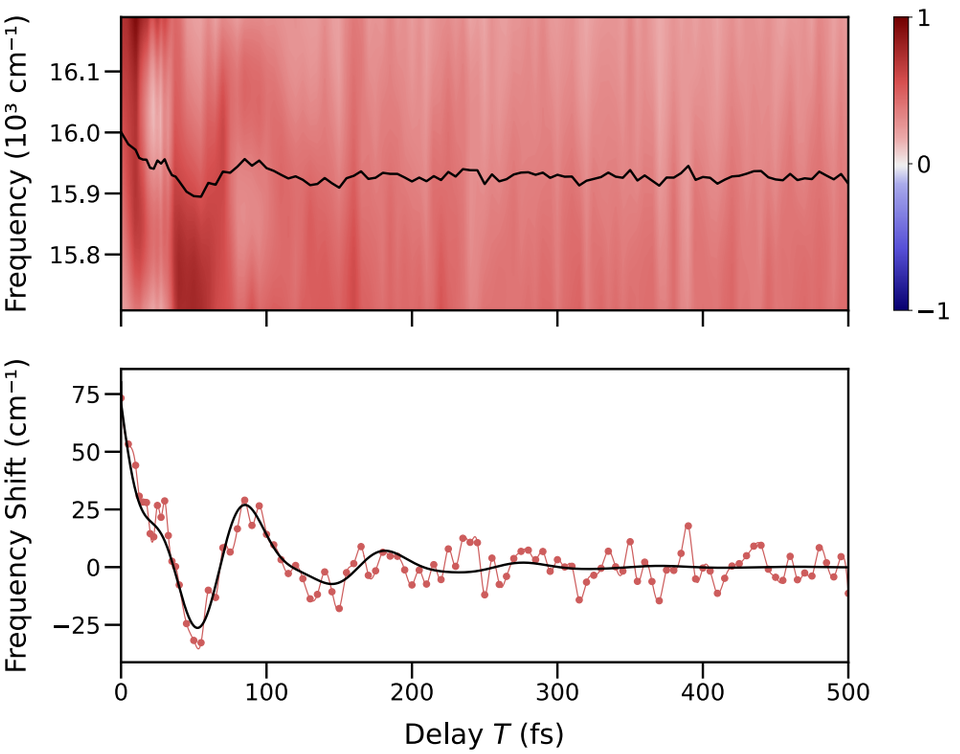

FIG. 9. Time evolution of the average frequency of the below-diagonal cross peak in the 2DES spectrum of NpF2164g5, as determined by a first-moment (FM) analysis, Eq. 1. *Top panel*: Heat map of the amplitude of the below-diagonal cross peak in the 2DES spectrum with respect to the detection frequency and the time delay T, with averaging over the 16400 ± 250-cm^{-1} range of the excitation axis. The FM of the cross peak with respect to the detection frequency over the 15950 ± 250-cm^{-1} range is plotted as a black trace. *Bottom panel*: Relative shift of the FM (red dots), with a model (black curve) consisting of the sum of a Gaussian decay and two damped cosinusoids. The model parameters are provided in the Supplementary Materials as Table IX.

spectroscopy was used recently to detect the relaxation of the active site over the fs–ps timescale of the bathy bacteriophytochrome PaBphP in terms of a red-to-blue dynamic Stokes shift of fluorescence from the biliverdin IXα chromophore.[112]

Over the subsequent $T > 50$-fs range, the FM response then exhibits an underdamped oscillation at 360 cm^{-1} and 680 cm^{-1} due to the out-of-plane bending and torsional modes of the methine linkage, respectively. These modes might be expected to contribute to the FM response because they would modulate the permanent dipole moment of the PCB chromophore by moving the D ring relative to the rest of the π-conjugated backbone, but the absence of the 800-cm^{-1} HOOP

mode from the principal components is interesting. We suggest that this is a filtering of the vibrational coherences in the FM response owing to an indirect detection via the permanent dipole moment. A comparable behavior was noted previously for the response of the nodal line in 2DES spectra by Jonas and coworkers in a study of the cyanine dye IR144.[48,113] The overall damping time of the FM modulations is ~60 fs, slower than observed for the rapidly damped coherences in the amplitude transients. The contribution of vibrational coherences of the solvation response detected in other systems has been discussed previously in 3PEPS experiments[114] and in the excitation energy dependence of 2DES amplitudes.[115]

IV. CONCLUSIONS

Despite the near mirror symmetry of the linear absorption and fluorescence spectra, the multidimensional electronic spectroscopy results presented here provide clear evidence for the formation of a distorted excited-state intermediate structure of the PCB chromophore in NpF2164g5 on an ultrafast timescale after optical excitation in terms of a below-diagonal cross peak and rapidly damped vibronic coherences. The ICT character of the intermediate is consistent with an assignment to a twisted and bent conformation of the methine bridge between the C and D rings of the PCB chromophore with a charge-separated, zwitterionic character.[7,90] This structure would arise from an ultrafast transfer of a π electron across the C15=C16 double bond as the D ring rotates out-of-plane, which would partially neutralize the positive charge delocalized over the A, B, and C rings,[38,116,117] rendering them more hydrophobic. The twisting of the C15=C16 bond and the out-of-plane deformation of the D ring towards a pyramidal C15 carbon would be expected to occur concurrently, as is observed in simulations of similar excited-state motions of a protonated Schiff base model for retinal in rhodopsin.[9] A comparable structure with ICT character would be expected prior to the excited-state barrier along the reaction coordinate

for the 15*E*/15*Z* photoisomerization of ring D in the photoactive CBCRs and in the phytochromes.

The global model shows that extensive spectral broadening with respect to the antidiagonal of the 2DES spectrum accompanies the developing cross peak, which reports that memory of the ground-to-excited-state energy gap of the optically prepared S_1 state of the PCB chromophore is lost owing to the change in electronic structure accompanying the formation of the product ICT state. Further, damping of the 350-cm^{-1} and 800-cm^{-1} coherences occurs essentially on the same timescale as that for conversion to the ICT state. This observation supports the conclusion that the ICT state is formed by a coherent nonadiabatic mechanism, involving passage through a CI between the S_1 state and the ICT state. Although the ultrafast damping of the 350-cm^{-1} and 800-cm^{-1} coherences suggests that these vibrations promote the formation of the ICT state, the FM response shows that at least two of the chromophore's vibrational motions modulate the permanent dipole moment of the PCB chromophore. The initial displacement from the Franck–Condon structure involves the full set of resonance Raman-active modes that were detected in the analysis of the vibrational structure of the linear absorption and fluorescence spectra, but it is likely that the ICT character develops over a very short timescale, requiring only small deformations[90,91] with respect to the out-of-plane coordinates. The observation that the FM transient's underdamped modulation is damped somewhat more slowly than the 350-cm^{-1} and 800-cm^{-1} coherences is not currently understood, but it deserves additional attention in simulations to determine if additional information on the mechanism for the electrostatic coupling of the chromophore and the surroundings can be obtained.

The dynamical picture for the response of the PCB chromophore in NpF2164g5 depicted in Fig. 8 would be expected to underlie the rate and quantum yield of the first step in the *Z* to *E* ring-flipping photoisomerization of the methine bridge between rings C and D in photoactive CBCRs, such as NpR6012g4. The local barrier on the potential energy surface of S_1/Z traps the ICT intermediate in the case

of NpF2164g5. As noted in the Introduction, the G632V and L714F mutations of NpR6012g4 apparently increase the height of the barrier by imposing packing hindrances to the out-of-plane motion of ring D, as implied by the proximity of these mutation sites shown in Fig. 1. In addition to the structural changes noted earlier that accompany replacement of the imidazole side chain of H688 with the phenol side chain of tyrosine, we suggest that the H688Y mutation further increases the height of the photoactivation barrier by lowering the polarization of the π-electron density along the delocalized backbone of the PCB chromophore. The orientation of the permanent dipole moment of the imidazole group[118] is roughly aligned with the direction of the π-electron conjugation of the C and D rings, which might favor the formation of a zwitterionic electronic configuration at the barrier. The phenol side chain of tyrosine is significantly less polar and the direction of the permanent dipole moment is rotated away; the dipole moments are <1.7 D[119] and ~4 D,[118,120] respectively. These ideas suggest that formation of the ICT state is a crucial intermediate step along the ring-flipping reaction coordinate leading to the product 15*E* configuration of the PCB chromophore. An additional implication is that the protein's reorganizational response to the formation and decay of the ICT character of the PCB chromophore contributes to the color and intensity sensitivity of the photoreceptor response in CBCRs and phytochromes. This hypothesis might be examined by observations of the FM response over the ps timescale for the crossing of the barrier leading to the 15*E* photoproduct.

SUPPLEMENTARY MATERIAL

The Supplementary Material includes the following: MIIPS SHG-FROG spectrogram and interferometric autocorrelation signals; residual phase spectra of the pump and probe excitation pulses; 2DES spectra of methylene blue in water and of water blanks; variable temperature survey of the linear absorption spectrum of NpF2164g5; MBO model parameters for the absorption and fluorescence spectra at 80 K and 298 K;

EADS spectrum for a 1D global model of the 2DES spectrum; 3DES FT vibronic spectrum; LPSVD model parameters for the modulated transients sampled from the 2DES spectrum and from the FM transient.

ACKNOWLEDGMENT

Work in the laboratories of WFB and of NCR was supported by grant awards DE-SC0010847 and DE-SC0002395, respectively, from the Photosynthetic Systems program of the Office of Basic Energy Sciences, U.S. Department of Energy. We thank Professor J. Clark Lagarias (University of California, Davis) for helpful comments on the manuscript.

DATA AND CODE AVAILABILITY

The data sets and code used to analyze the results reported in this paper will be available in an archive at the following DOI: 10.5281/zenodo.XXXXXXX.

COMPETING INTERESTS

The authors declare no competing interests associated with this work.

AUTHOR CONTRIBUTIONS

CHL and WFB conceived the study and organized the project, with WFB providing overall supervision. WFB obtained funding for the project. CHL carried out the experiments and analyzed the data sets. CHL and WFB contributed the overall interpretation of the experimental results. The manuscript was written by WFB and CHL, aided by comments by NCR.

REFERENCES

[1]S. L. Logunov, L. Song, and M. A. El-Sayed, "Excited-state dynamics of a protonated retinal schiff base in solution," J. Phys. Chem. **100**, 18586–18591 (1996).

[2]A. Sanchez-Galvez, P. Hunt, M. A. Robb, M. Olivucci, T. Vreven, and H. B. Schlegel, "Ultrafast radiationless deactivation of organic dyes: Evidence for a two-state two-mode pathway in polymethine cyanines," J. Am. Chem. Soc. **122**, 2911–2924 (2000).

[3]A. Cembran, F. Bernardi, M. Olivucci, and M. Garavelli, "The retinal chromophore/chloride ion pair: structure of the photoisomerization path and interplay of charge transfer and covalent states," Proc. Natl. Acad. Sci. U. S. A. **102**, 6255–6260 (2005).

[4]W. F. Beck, M. M. Bishop, J. D. Roscioli, S. Ghosh, and H. A. Frank, "Excited state conformational dynamics in carotenoids: dark intermediates and excitation energy transfer," Arch. Biochem. Biophys. **572**, 175–183 (2015).

[5]B. G. Levine and T. J. Martínez, "Isomerization through conical intersections," Annu. Rev. Phys. Chem. **58**, 613–634 (2007).

[6]B. G. Levine and T. J. Martínez, "Ab initio multiple spawning dynamics of excited butadiene: role of charge transfer," J. Phys. Chem. A **113**, 12815–12824 (2009).

[7]V. Bonačić-Koutecký, J. Koutecký, and J. Michl, "Neutral and charged biradicals, zwitterions, funnels in S_1, and proton translocation: Their role in photochemistry, photophysics, and vision," Angew. Chem., Int. Ed. Engl. **26**, 170–189 (1987).

[8]J. Michl and V. Bonačić-Koutecký, *Electronic Aspects of Organic Photochemistry* (Wiley, New York, 1990).

[9]J. P. Malhado, R. Spezia, and J. T. Hynes, "Dynamical friction effects on the photoisomerization of a model protonated schiff base in solution," J. Phys. Chem. A **115**, 3720–3735 (2011).

[10]J. B. Rose, J. A. Gascón, D. I. Sheppard, C. A. Kerfeld, and W. F. Beck, "Photoactivation transition state and dynamical response of the orange carotenoid

protein," J. Phys. Chem. B **129**, 12841–12852 (2025).

[11]N. C. Rockwell, S. S. Martin, and J. C. Lagarias, "Red/green cyanobacteriochromes: sensors of color and power," Biochemistry **51**, 9667–9677 (2012).

[12]S. Osoegawa, R. Miyoshi, K. Watanabe, Y. Hirose, T. Fujisawa, M. Ikeuchi, and M. Unno, "Identification of the deprotonated pyrrole nitrogen of the bilin-based photoreceptor by Raman spectroscopy with an advanced computational analysis," J. Phys. Chem. B **123**, 3242–3247 (2019).

[13]K. Fushimi and R. Narikawa, "Cyanobacteriochromes: photoreceptors covering the entire UV-to-visible spectrum," Curr. Opin. Struct. Biol. **57**, 39–46 (2019).

[14]N. C. Rockwell and J. C. Lagarias, "Cyanobacteriochromes: A rainbow of photoreceptors," Annu. Rev. Microbiol. **78**, 61–81 (2024).

[15]N. C. Rockwell and J. C. Lagarias, "Circular dichroism spectroscopy reveals multiple phytochrome photoproducts in equilibrium," Photochem. Photobiol. Sci. **24**, 1351–1371 (2025).

[16]N. C. Rockwell, S. S. Martin, K. Feoktistova, and J. C. Lagarias, "Diverse two-cysteine photocycles in phytochromes and cyanobacteriochromes," Proc. Natl. Acad. Sci. U. S. A. **108**, 11854–11859 (2011).

[17]N. C. Rockwell, S. S. Martin, A. G. Gulevich, and J. C. Lagarias, "Phycoviolobilin formation and spectral tuning in the DXCF cyanobacteriochrome subfamily," Biochemistry **51**, 1449–1463 (2012).

[18]P. W. Kim, L. H. Freer, N. C. Rockwell, S. S. Martin, J. C. Lagarias, and D. S. Larsen, "Femtosecond photodynamics of the red/green cyanobacteriochrome NpR6012g4 from *Nostoc punctiforme*. 1. Forward dynamics," Biochemistry **51**, 608–618 (2012).

[19]P. W. Kim, L. H. Freer, N. C. Rockwell, S. S. Martin, J. C. Lagarias, and D. S. Larsen, "Second-chance forward isomerization dynamics of the red/green cyanobacteriochrome NpR6012g4 from *Nostoc punctiforme*," J. Am. Chem. Soc. **134**, 130–133 (2012).

[20]P. W. Kim, J. Pan, N. C. Rockwell, C.-W. Chang, K. C. Taylor, J. C. Lagarias, and D. S. Larsen, "Ultrafast E to Z photoisomerization dynamics of the Cph1 phytochrome,"

Chem. Phys. Lett. **549**, 86–92 (2012).

[21]S. M. Gottlieb, P. W. Kim, C.-W. Chang, S. J. Hanke, R. J. Hayer, N. C. Rockwell, S. S. Martin, J. C. Lagarias, and D. S. Larsen, "Conservation and diversity in the primary forward photodynamics of red/green cyanobacteriochromes," Biochemistry **54**, 1028–1042 (2015).

[22]X. Xu, A. Port, C. Wiebeler, K.-H. Zhao, I. Schapiro, and W. Gärtner, "Structural elements regulating the photochromicity in a cyanobacteriochrome," Proc. Natl. Acad. Sci. U. S. A. **117**, 2432–2440 (2020).

[23]S. Lim, Q. Yu, S. M. Gottlieb, C.-W. Chang, N. C. Rockwell, S. S. Martin, D. Madsen, J. C. Lagarias, D. S. Larsen, and J. B. Ames, "Correlating structural and photochemical heterogeneity in cyanobacteriochrome NpR6012g4," Proc. Natl. Acad. Sci. U. S. A. **115**, 4387–4392 (2018).

[24]N. C. Rockwell, S. S. Martin, S. Lim, J. C. Lagarias, and J. B. Ames, "Characterization of red/green cyanobacteriochrome NpR6012g4 by solution nuclear magnetic resonance spectroscopy: A hydrophobic pocket for the C15-E,anti chromophore in the photoproduct," Biochemistry **54**, 3772–3783 (2015).

[25]A. J. Jenkins, S. M. Gottlieb, C.-W. Chang, R. J. Hayer, S. S. Martin, J. C. Lagarias, and D. S. Larsen, "Conservation and diversity in the secondary forward photodynamics of red/green cyanobacteriochromes," Photochem. Photobiol. Sci. **18**, 2539–2552 (2019).

[26]J. Dasgupta, R. R. Frontiera, K. C. Taylor, J. C. Lagarias, and R. A. Mathies, "Ultrafast excited-state isomerization in phytochrome revealed by femtosecond stimulated Raman spectroscopy," Proc. Natl. Acad. Sci. U. S. A. **106**, 1784–1789 (2009).

[27]P. W. Kim, N. C. Rockwell, S. S. Martin, J. C. Lagarias, and D. S. Larsen, "Dynamic inhomogeneity in the photodynamics of cyanobacterial phytochrome Cph1," Biochemistry **53**, 2818–2826 (2014).

[28]V. Sineshchekov, J. Mailliet, G. Psakis, K. Feilke, J. Kopycki, M. Zeidler, L.-O. Essen, and J. Hughes, "Tyrosine 263 in cyanobacterial phytochrome Cph1 optimizes photochemistry at the prelumi-R→lumi-R step," Photochem. Photobiol. **90**, 786–795

(2014).

[29]S. Nagano, C. Song, V. Rohr, M. J. Mackintosh, O. T. Hoang, A. Kraskov, Y. Yang, J. Hughes, K. Heyne, M.-A. Mroginski, I. Schapiro, and P. Hildebrandt, "Integrated study of fluorescence enhancement in the Y176H variant of cyanobacterial phytochrome Cph1," Biochemistry **64**, 1348–1358 (2025).

[30]K. M. Spillane, J. Dasgupta, and R. A. Mathies, "Conformational homogeneity and excited-state isomerization dynamics of the bilin chromophore in phytochrome Cph1 from resonance Raman intensities," Biophys. J. **102**, 709–717 (2012).

[31]P. W. Kim, N. C. Rockwell, L. H. Freer, C.-W. Chang, S. S. Martin, J. C. Lagarias, and D. S. Larsen, "Unraveling the primary isomerization dynamics in cyanobacterial phytochrome Cph1 with multi-pulse manipulations," J. Phys. Chem. Lett. **4**, 2605–2609 (2013).

[32]C.-W. Chang, S. M. Gottlieb, P. W. Kim, N. C. Rockwell, J. C. Lagarias, and D. S. Larsen, "Reactive ground-state pathways are not ubiquitous in red/green cyanobacteriochromes," J. Phys. Chem. B **117**, 11229–11238 (2013).

[33]L. A. Bizimana, J. Epstein, J. Brazard, and D. B. Turner, "Conformational homogeneity in the P_r isomer of phytochrome Cph1," J. Phys. Chem. B **121**, 2622–2630 (2017).

[34]L. A. Bizimana, C. A. Farfan, J. Brazard, and D. B. Turner, "E to Z photoisomerization of phytochrome Cph1Δ exceeds the Born–Oppenheimer adiabatic limit," J. Phys. Chem. Lett. **10**, 3550–3556 (2019).

[35]C. Wang, M. L. Flanagan, R. D. McGillicuddy, H. Zheng, A. R. Ginzburg, X. Yang, K. Moffat, and G. S. Engel, "Bacteriophytochrome photoisomerization proceeds homogeneously despite heterogeneity in ground state," Biophys. J. **111**, 2125–2134 (2016).

[36]N. C. Rockwell, M. V. Moreno, S. S. Martin, and J. C. Lagarias, "Protein-chromophore interactions controlling photoisomerization in red/green cyanobacteriochromes," Photochem. Photobiol. Sci. **21**, 471–491 (2022).

[37]R. Narikawa, T. Ishizuka, N. Muraki, T. Shiba, G. Kurisu, and M. Ikeuchi, "Structures of cyanobacteriochromes from phototaxis regulators AnPixJ and TePixJ reveal general and specific photoconversion mechanism," Proc. Natl. Acad. Sci. U. S. A. **110**, 918–923 (2013).

[38]N. C. Rockwell, S. S. Martin, S. Lim, J. C. Lagarias, and J. B. Ames, "Characterization of red/green cyanobacteriochrome NpR6012g4 by solution nuclear magnetic resonance spectroscopy: A protonated bilin ring system in both photostates," Biochemistry **54**, 2581–2600 (2015).

[39]N. J. Hestand and F. C. Spano, "Expanded theory of H- and J-molecular aggregates: The effects of vibronic coupling and intermolecular charge transfer," Chem. Rev. **118**, 7069–7163 (2018).

[40]G. A. Gambetta and J. C. Lagarias, "Genetic engineering of phytochrome biosynthesis in bacteria," Proc. Natl. Acad. Sci. U. S. A. **98**, 10566–10571 (2001).

[41]J. K. Gurchiek, J. B. Rose, M. J. Guberman-Pfeffer, R. W. Tilluck, S. Ghosh, J. A. Gascón, and W. F. Beck, "Fluorescence anisotropy detection of barrier crossing and ultrafast conformational dynamics in the S_2 state of β-carotene," J. Phys. Chem. B **124**, 9029–9046 (2020).

[42]J. B. Rose, J. A. Gascón, M. Sutter, D. I. Sheppard, C. A. Kerfeld, and W. F. Beck, "Photoactivation of the orange carotenoid protein requires two light-driven reactions mediated by a metastable monomeric intermediate," Phys. Chem. Chem. Phys. **25**, 33000–33012 (2023).

[43]R. W. Tilluck, S. Ghosh, M. J. Guberman-Pfeffer, J. D. Roscioli, J. K. Gurchiek, A. M. LaFountain, H. A. Frank, J. A. Gascón, and W. F. Beck, "Interexciton nonradiative relaxation pathways in the peridinin-chlorophyll protein," Cell Reports Phys. Sci. **2**, 100380 (2021).

[44]N. Mohan T. M., C. H. Leslie, S. Sil, J. B. Rose, R. W. Tilluck, and W. F. Beck, "Broadband 2DES detection of vibrational coherence in the S_x state of canthaxanthin," J. Chem. Phys. **155**, 035103 (2021).

[45]S. H. Shim and M. T. Zanni, "How to turn your pump-probe instrument into a multidimensional spectrometer: 2D IR and vis spectroscopies via pulse shaping," Phys. Chem. Chem. Phys. **11**, 748–761 (2009).

[46]R. Augulis and D. Zigmantas, "Two-dimensional electronic spectroscopy with double modulation lock-in detection: enhancement of sensitivity and noise resistance," Opt. Express **19**, 13126–13133 (2011).

[47]J. D. Hybl, A. W. Albrecht, S. M. Gallagher Faeder, and D. M. Jonas, "Two-dimensional electronic spectroscopy," Chem. Phys. Lett. **297**, 307–313 (1998).

[48]D. M. Jonas, "Two-dimensional femtosecond spectroscopy," Annu. Rev. Phys. Chem. **54**, 425–463 (2003).

[49]L. Lepetit, G. Chériaux, and M. Joffre, "Linear techniques of phase measurement by femtosecond spectral interferometry for applications in spectroscopy," J. Opt. Soc. Am. B **12**, 2467–2474 (1995).

[50]D. B. Turner, K. E. Wilk, P. M. G. Curmi, and G. D. Scholes, "Comparison of electronic and vibrational coherence measured by two-dimensional electronic spectroscopy," J. Phys. Chem. Lett. **2**, 1904–1911 (2011).

[51]J. A. Myers, K. L. M. Lewis, P. F. Tekavec, and J. P. Ogilvie, "Two-color two-dimensional Fourier transform electronic spectroscopy with a pulse-shaper," Opt. Express **16**, 17420–17428 (2008).

[52]V. V. Lozovoy, I. Pastirk, and M. Dantus, "Multiphoton intrapulse interference 4: characterization and compensation of the spectral phase of ultrashort laser pulses," Opt. Lett. **29**, 775–777 (2004).

[53]K. W. DeLong, R. Trebino, J. Hunter, and W. E. White, "Frequency-resolved optical gating with the use of second-harmonic generation," J. Opt. Soc. Am. B **11**, 2206–2215 (1994).

[54]H. Barkhuijsen, R. Beer, and D. Ormondt, "Improved algorithm for noniterative time-domain model fitting to exponentially damped magnetic resonance signals," J. Magn. Reson. **73**, 553–557 (1987).

[55]F. Wise, M. Rosker, G. Millhauser, and C. Tang, "Application of linear prediction least-squares fitting to time-resolved optical spectroscopy," IEEE J. Quantum Electron. **23**, 1116–1121 (1987).

[56]I. Eom, E. Yoon, S.-H. Baik, Y.-S. Lim, and T. Joo, "Retrieval of frequency spectrum from time-resolved spectroscopic data: comparison of Fourier transform and linear prediction methods," Opt. Express **22**, 30512–30519 (2014).

[57]L. Zhu, P. Li, M. Huang, J. T. Sage, and P. M. Champion, "Real time observation of low frequency heme protein vibrations using femtosecond coherence spectroscopy," Phys. Rev. Lett. **72**, 301–304 (1994).

[58]F. Rosca, A. T. N. Kumar, X. Ye, T. Sjodin, A. A. Demidov, and P. M. Champion, "Investigations of coherent vibrational oscillations in myoglobin," J. Phys. Chem. A **104**, 4280–4290 (2000).

[59]S. Mukamel, *Principles of Nonlinear Optical Spectroscopy* (Oxford University Press, New York, 1995).

[60]G. R. Fleming and M. Cho, "Chromophore-solvent dynamics," Annu. Rev. Phys. Chem. **47**, 109–134 (1996).

[61]S. Ghosh, M. M. Bishop, J. D. Roscioli, J. J. Mueller, N. C. Shepherd, A. M. LaFountain, H. A. Frank, and W. F. Beck, "Femtosecond heterodyne transient-grating studies of nonradiative decay of the S_2 ($1^1B_u^+$) state of β-carotene: Contributions from dark intermediates and double-quantum coherences," J. Phys. Chem. B **119**, 14905–14924 (2015).

[62]J. K. Gurchiek, H. Bao, M. A. Domínguez-Martín, S. E. McGovern, C. E. Marquardt, J. D. Roscioli, S. Ghosh, C. A. Kerfeld, and W. F. Beck, "Fluorescence and excited-state conformational dynamics of the orange carotenoid protein," J. Phys. Chem. B **122**, 1792–1800 (2018).

[63]J. M. Hollas and P. F. Taday, "Methyl and vinyl torsional potential functions in 4-methylstyrene from supersonic jet fluorescence spectroscopy," J. Chem. Soc. Faraday Trans. **86**, 217 (1990).

[64]J. Michael Hollas and P. F. Taday, "Methyl and vinyl torsional potentials in *cis*- and *trans*-3-methylstyrene from supersonic jet fluorescence spectra," J Chem Soc Faraday Trans **87**, 3585–3593 (1991).

[65]J. M. Granadino-Roldán, M. Fernández-Gómez, and A. Navarro, "The vibrational analysis of styrene, revisited," Chem. Phys. Lett. **372**, 255–262 (2003).

[66]S. P. Fodor, J. C. Lagarias, and R. A. Mathies, "Resonance Raman analysis of the P_r and P_{fr} forms of phytochrome," Biochemistry **29**, 11141–11146 (1990).

[67]S. R. Tachibana, L. Tang, C. Chen, L. Zhu, Y. Takeda, K. Fushimi, T. K. Seevers, R. Narikawa, M. Sato, and C. Fang, "Transient electronic and vibrational signatures during reversible photoswitching of a cyanobacteriochrome photoreceptor," Spectrochim. Acta A Mol. Biomol. Spectrosc. **250**, 119379 (2021).

[68]D. Buhrke, G. Battocchio, S. Wilkening, M. Blain-Hartung, T. Baumann, F.-J. Schmitt, T. Friedrich, M.-A. Mroginski, and P. Hildebrandt, "Red, orange, green: Light- and temperature-dependent color tuning in a cyanobacteriochrome," Biochemistry **59**, 509–519 (2020).

[69]H. Kano and T. Kobayashi, "Real-time spectroscopy of frenkel exciton system," J. Lumin. **100**, 269–282 (2002).

[70]L. A. Bizimana, W. P. Carbery, T. A. Gellen, and D. B. Turner, "Signatures of herzberg-teller coupling in three-dimensional electronic spectroscopy," J. Chem. Phys. **146**, 084311 (2017).

[71]P. P. Roy, S. Kundu, N. Makri, and G. R. Fleming, "Interference between franck-condon and herzberg-teller terms in the condensed-phase molecular spectra of metal-based tetrapyrrole derivatives," J. Phys. Chem. Lett. **13**, 7413–7419 (2022).

[72]I. H. M. van Stokkum, D. S. Larsen, and R. van Grondelle, "Global and target analysis of time-resolved spectra," Biochim. Biophys. Acta **1657**, 82–104 (2004).

[73]R. R. Riter, M. D. Edington, and W. F. Beck, "Protein-matrix solvation dynamics in the α subunit of C-phycocyanin," J. Phys. Chem. **100**, 14198–14205 (1996).

[74]W. T. Pollard, S. Lee, and R. A. Mathies, "Wave packet theory of dynamic absorption spectra in femtosecond pump–probe experiments," J. Chem. Phys. **92**, 4012–4029

(1990).

[75]W. T. Pollard and R. A. Mathies, "Analysis of femtosecond dynamic absorption spectra of nonstationary states," Annu. Rev. Phys. Chem. **43**, 497–523 (1992).

[76]V. Butkus, D. Zigmantas, L. Valkunas, and D. Abramavicius, "Vibrational vs. electronic coherences in 2D spectrum of molecular systems," Chem. Phys. Lett. **545**, 40–43 (2012).

[77]D. Egorova, "Self-analysis of coherent oscillations in time-resolved optical signals," J. Phys. Chem. A **118**, 10259–10267 (2014).

[78]C. A. Farfan and D. B. Turner, "Interference among multiple vibronic modes in Two-Dimensional electronic spectroscopy," Mathematics **8**, 157 (2020).

[79]D. Paleček, P. Edlund, S. Westenhoff, and D. Zigmantas, "Quantum coherence as a witness of vibronically hot energy transfer in bacterial reaction center," Sci. Adv. **3**, e1603141 (2017).

[80]K. Yang, N. Mohan T. M., J. B. Rose, C. H. Leslie, M. Sutter, C. A. Kerfeld, and W. F. Beck, "Spectral broadening and vibronic dynamics of the S_2 state of canthaxanthin in the orange carotenoid protein," J. Chem. Phys. **161**, 155101 (2024).

[81]D. R. Yarkony, "Conical intersections: The new conventional wisdom," J. Phys. Chem. A **105**, 6277–6293 (2001).

[82]J. Michl, "Historical introduction," in *Conical Intersections: Electronic Structure, Dynamics & Spectroscopy*, edited by W. Domcke, D. Yarkony, and H. Köppel (World Scientific, Singapore, 2004) pp. ix–xiii.

[83]J. Brazard, L. A. Bizimana, T. Gellen, W. P. Carbery, and D. B. Turner, "Experimental detection of branching at a conical intersection in a highly fluorescent molecule," J. Phys. Chem. Lett. **7**, 14–19 (2016).

[84]S. Gozem, H. L. Luk, I. Schapiro, and M. Olivucci, "Theory and simulation of the ultrafast double-bond isomerization of biological chromophores," Chem. Rev. **117**, 13502–13565 (2017).

[85]B. G. Levine, M. P. Esch, B. S. Fales, D. T. Hardwick, W.-T. Peng, and Y. Shu, "Conical intersections at the nanoscale: Molecular ideas for materials," Annu. Rev. Phys.

Chem. **70**, 21–43 (2019).

[86]S. Sil, R. W. Tilluck, N. Mohan T M, C. H. Leslie, J. B. Rose, M. A. Domínguez-Martín, W. Lou, C. A. Kerfeld, and W. F. Beck, "Excitation energy transfer and vibronic coherence in intact phycobilisomes," Nat. Chem. **14**, 1286–1294 (2022).

[87]W. F. Beck, "Intramolecular charge transfer and the function of vibronic excitons in photosynthetic light harvesting," Photosynth. Res. **162**, 139–156 (2024).

[88]R. W. Tilluck, N. Mohan T M, C. V. Hetherington, C. H. Leslie, S. Sil, J. Frazier, M. Zhang, B. G. Levine, P. G. Van Patten, and W. F. Beck, "Vibronic excitons and conical intersections in semiconductor quantum dots," J. Phys. Chem. Lett. **12**, 9677–9683 (2021).

[89]C. V. Hetherington, N. Mohan T M, R. W. Tilluck, W. F. Beck, and B. G. Levine, "Origin of vibronic coherences during carrier cooling in colloidal quantum dots," J. Phys. Chem. Lett. **14**, 11651–11658 (2023).

[90]V. Bonačić-Koutecký, P. Bruckmann, P. Hiberty, J. Koutecký, C. Leforestier, and L. Salem, "Sudden polarization in the zwitterionic Z_1 excited states of organic intermediates. photochemical implications," Angew. Chem., Int. Ed. Engl. **14**, 575–576 (1975).

[91]L. Salem, "The sudden polarization effect and its possible role in vision," Acc. Chem. Res. **12**, 87–92 (1979).

[92]M. Klessinger and J. Michl, *Excited States and Photochemistry of Organic Molecules* (Wiley-VCH Verlag, 1995).

[93]G. J. Atchity, S. S. Xantheas, and K. Ruedenberg, "Potential energy surfaces near intersections," J. Chem. Phys. **95**, 1862–1876 (1991).

[94]H.-G. Duan, R. J. D. Miller, and M. Thorwart, "Impact of vibrational coherence on the quantum yield at a conical intersection," J. Phys. Chem. Lett. **7**, 3491–3496 (2016).

[95]S. R. Rather and G. D. Scholes, "From fundamental theories to quantum coherences in electron transfer," J. Am. Chem. Soc. **141**, 708–722 (2019).

[96]S. R. Rather, G. D. Scholes, and L. X. Chen, "From coherence to function: Exploring the connection in chemical systems," Acc. Chem. Res. **57**, 2620–2630 (2024).

[97]Y. Wang, A. Benny, B. Le Dé, A. W. Chin, and G. D. Scholes, "A numerically exact description of ultrafast vibrational decoherence in vibration-coupled electron transfer," Proc. Natl. Acad. Sci. U. S. A. **122**, e2416542122 (2025).

[98]A. Mitra, "Quantum quench dynamics," Annu. Rev. Condens. Matter Phys. **9**, 245–259 (2018).

[99]P. Kukura, D. W. McCamant, S. Yoon, D. B. Wandschneider, and R. A. Mathies, "Structural observation of the primary isomerization in vision with femtosecond-stimulated Raman," Science **310**, 1006–1009 (2005).

[100]P. J. M. Johnson, A. Halpin, T. Morizumi, V. I. Prokhorenko, O. P. Ernst, and R. J. D. Miller, "Local vibrational coherences drive the primary photochemistry of vision," Nat. Chem. **7**, 980 (2015).

[101]P. J. M. Johnson, M. H. Farag, A. Halpin, T. Morizumi, V. I. Prokhorenko, J. Knoester, T. L. Jansen, O. P. Ernst, and R. Miller, "The primary photochemistry of vision occurs at the molecular speed limit," J. Phys. Chem. B **121**, 4040–4047 (2017).

[102]I. Ghosh, Q. Shen, P.-J. E. Wu, and G. S. Engel, "Vibronic conical intersection trajectory signatures in wave packet coherences," J. Phys. Chem. Lett. **15**, 12494–12500 (2024).

[103]P. Kukura, D. W. McCamant, and R. A. Mathies, "Femtosecond time-resolved stimulated Raman spectroscopy of the S_2 ($1B_u^+$) excited state of β-carotene," J. Phys. Chem. A **108**, 5921–5925 (2004).

[104]B. J. Homoelle, M. D. Edington, W. M. Diffey, and W. F. Beck, "Stimulated photon-echo and transient-grating studies of protein-matrix solvation dynamics and interexciton-state radiationless decay in α phycocyanin and allophycocyanin," J. Phys. Chem. B **102**, 3044–3052 (1998).

[105]X. J. Jordanides, M. J. Lang, X. Song, and G. R. Fleming, "Solvation dynamics in protein environments studied by photon echo spectroscopy," J. Phys. Chem. B **103**, 7995–8005 (1999).

[106]S. Lampa-Pastirk and W. F. Beck, "Polar solvation dynamics in Zn(II)-substituted cytochrome *c*: Diffusive sampling of the energy landscape in the hydrophobic core and solvent-contact layer," J. Phys. Chem. B **108**, 16288–16294 (2004).

[107]Y. Qin, L. Wang, and D. Zhong, "Dynamics and mechanism of ultrafast water-protein interactions," Proc. Natl. Acad. Sci. U. S. A. **113**, 8424–8429 (2016).

[108]T. Joo, Y. Jia, J.-Y. Yu, D. Jonas, and G. Fleming, "Dynamics in isolated bacterial light harvesting antenna (LH2) of *Rhodobacter sphaeroides* at room temperature," The Journal of Physical Chemistry **100**, 2399–2409 (1996).

[109]K. F. Everitt, E. Geva, and J. L. Skinner, "Determining the solvation correlation function from three-pulse photon echoes in liquids," J. Chem. Phys. **114**, 1326–1335 (2001).

[110]T. Joo, Y. Jia, J.-Y. Yu, M. J. Lang, and G. R. Fleming, "Third-order nonlinear time domain probes of solvation dynamics," J. Chem. Phys. **104**, 6089–6108 (1996).

[111]J. Tripathy, J. J. Mueller, N. C. Shepherd, and W. F. Beck, "Dynamic solvation and coupling of the hydration shell of Zn^{II}-substituted cytochrome *c* in the presence of guanidinium ions," J. Phys. Chem. B **117**, 14589–14598 (2013).

[112]D. Wang, Y. Qin, M. Zhang, X. Li, L. Wang, X. Yang, and D. Zhong, "The origin of ultrafast multiphasic dynamics in photoisomerization of bacteriophytochrome," J. Phys. Chem. Lett. **11**, 5913–5919 (2020).

[113]J. D. Hybl, A. Yu, D. A. Farrow, and D. M. Jonas, "Polar solvation dynamics in the femtosecond evolution of two-dimensional Fourier transform spectra," J. Phys. Chem. A **106**, 7651–7654 (2002).

[114]N. Christensson, B. Dietzek, A. Yartsev, and T. Pullerits, "Solute specific polar solvation studied by photon echo spectroscopy," Chem. Phys. **357**, 85–95 (2009).

[115]J. Lu, Y. Lee, and J. M. Anna, "Extracting the frequency-dependent dynamic stokes shift from two-dimensional electronic spectra with prominent vibrational coherences," J. Phys. Chem. B **124**, 8857–8867 (2020).

[116]T. Noji, K. Saito, and H. Ishikita, "Molecular origins of absorption wavelength variation among phycocyanobilin-binding proteins," Biophys. J. **123**, 3375–3385

(2024).

[117]L. Köhler, W. Gärtner, G. Salvan, J. Matysik, C. Wiebeler, and C. Song, "Photocycle of a cyanobacteriochrome: a charge defect on ring C impairs conjugation in chromophore," Chem. Sci. **14**, 6295–6308 (2023).

[118]M. R. Ross, A. M. White, F. Yu, J. T. King, V. L. Pecoraro, and K. J. Kubarych, "Histidine orientation modulates the structure and dynamics of a de novo metalloenzyme active site," J. Am. Chem. Soc. **137**, 10164–10176 (2015).

[119]F. L. Tobiason, G. H. Cain, and J. W. Anderson, "Dipole moment characterization of phenol–, *o*-cresol–, and *p*-cresol–formaldehyde resins," J. Polym. Sci. Polym. Chem. Ed. **16**, 275–282 (1978).

[120]D. Christen, J. H. Griffiths, and J. Sheridan, "The microwave spectrum of imidazole; complete structure and the electron distribution from nuclear quadrupole coupling tensors and dipole moment orientation," Z. Naturforsch. A **36**, 1378–1385 (1981).